

HOSTED BY



ELSEVIER

Contents lists available at ScienceDirect

The Egyptian Journal of Remote Sensing and Space Sciences

journal homepage: www.sciencedirect.com

Research Paper

Spatial prediction and mapping of water quality of Owabi reservoir from satellite imageries and machine learning models[☆]Yvonne Yeboah Adusei^{a,*}, Jonathan Quaye-Ballard^b, Albert Amatey Adjaottor^a, Alex Appiah Mensah^c^a Department of Materials Engineering, College of Engineering, Kwame Nkrumah University of Science and Technology, Private Mail Bag, University Post Office, Kumasi, Ghana^b Department of Geomatic Engineering, College of Engineering, Kwame Nkrumah University of Science and Technology, Private Mail Bag, University Post Office, Kumasi, Ghana^c Department of Forest Resource Management, Faculty of Forest Sciences, Swedish University of Agricultural Sciences, Skogsmarksgränd, SE-90183 Umeå, Sweden

ARTICLE INFO

Article history:

Received 12 March 2021

Revised 30 April 2021

Accepted 20 June 2021

Available online 29 June 2021

Keywords:

Water quality

Optical satellite image data

Machine learning models

Owabi Reservoir

ABSTRACT

Estimation and mapping of surface water quality are vital for the planning and sustainable management of inland reservoirs. The study aimed at retrieving and mapping water quality parameters (WQPs) of Owabi Dam reservoir from Sentinel-2 (S2) and Landsat 8 (L8) satellite data, using random forests (RF), support vector machines (SVM) and multiple linear regression (MLR) models. Water samples from 45 systematic plots were analysed for pH, turbidity, alkalinity, total dissolved solids and dissolved oxygen. The performances of all three models were compared in terms of adjusted coefficient of determination (R^2_{adj}), and the root mean square error (RMSE) using repeated k-fold cross-validation procedure. To determine the status of water quality, pixel-level predictions were used to compute model-assisted estimates of WQPs and compared with reference values from the World Health Organization. Generally, all three models produced more accurate results for S2 compared to L8. On average, the inter-sensor relative efficiency showed that S2 outperformed L8 by 67% in retrieving WQPs of the Owabi Dam reservoir. S2 gave the highest accuracy for RF ($R^2_{adj} = 95\text{--}99\%$, RMSE = 0.02–3.03) and least for MLR ($R^2_{adj} = 55\text{--}91\%$, RMSE = 0.03–3.14). Compared to RF, SVM showed similar results for S2 but with slightly higher RMSEs (0.03–3.99). The estimated pH (7.06), total dissolved solids (39.19 mg/L) and alkalinity (179.60 mg/L) were within acceptable limits, except for turbidity (33.49 mg/L) which exceeded the reference thresholds. The S2 and RF models are recommended for the monitoring of surface water quality of the Owabi Dam reservoir.

© 2021 National Authority for Remote Sensing and Space Sciences. Production and hosting by Elsevier B.V. This is an open access article under the CC BY-NC-ND license (<http://creativecommons.org/licenses/by-nc-nd/4.0/>).

1. Introduction

Water is a key resource for humans and the environment (Marobhe et al., 2007). Globally, about 3% of the total water resource constitute freshwaters, but only 5% of the freshwaters is available for human use (Usharani et al., 2010). About 40% of the world's population is estimated to be experiencing water scarcity, a figure perceived to rise because of population growth. Human-induced environmental changes have threatened the quality of surface water thereby preventing the attainment of the United Nations Sustainable Development Goals on water quality (World Health Organization, 2004). In sub-Saharan Africa, about two million people die from water-borne diseases (Karikari et al., 2007).

Peer review under responsibility of National Authority for Remote Sensing and Space Sciences.

* Corresponding author.

E-mail address: yvonne.aduseiyeboah@yahoo.com (Y.Y. Adusei).

<https://doi.org/10.1016/j.ejrs.2021.06.006>

1110-9823/© 2021 National Authority for Remote Sensing and Space Sciences. Production and hosting by Elsevier B.V.

This is an open access article under the CC BY-NC-ND license (<http://creativecommons.org/licenses/by-nc-nd/4.0/>).

In Ghana, most of the waterbodies are suffering from high levels of pollution due to poor settlement planning, poor farming techniques and illegal small-scale mining activities (Ntow, 2001). The Owabi Dam, located in the Kumasi Metropolis provides about 20% of the domestic water and fishing livelihoods for the inhabitants (Boadi et al., 2018). The dam is fed by several other streams in the metropolis and usually carry waste materials which are emptied into the reservoir after a heavy downpour, causing high levels of water pollution and resulting in higher costs of water treatment by the Owabi Water Works (Badu et al., 2013). In addition, the presence of pollutants like heavy metals, pesticides and fertilizers from agricultural activities disrupts the aquatic ecosystem (Du Laing et al., 2009) and this results in high acidity content, increased sediment load and high concentration of chemical and harmful organisms which render the water unsafe for human consumption (United Nations world water assessment programme, 2009).

Previous studies have assessed the quality of surface water in Owabi Dam by looking at the physicochemical properties such as

changes in water quality as well as the heavy metal levels and nutrient loads (e.g. Akoto et al., 2008, 2017; Akoto and Abankwa, 2014; Boadi et al., 2018). Whilst these studies have used conventional field methods to estimate water quality in the reservoir, the use of remote sensing (RS) has rarely been explored for water quality estimation in the Owabi Dam.

Recent developments in RS technology have made available wall-to-wall auxiliary data to support the monitoring of terrestrial and aquatic resources (Saadi et al., 2014; Feyisa et al., 2014; Gholizadeh et al., 2016; Mollaei, 2018). For example, Abdelmalik (2018) estimated the inland water quality parameters (WQP) in north-eastern region of Egypt using Advanced Space-borne Thermal Emission and Reflection Radiation (ASTER) imageries, and Mollaei (2018) also demonstrated how phytoplankton chlorophyll concentration could be monitored in the Western Basin of Lake Erie using RS data. The use of Landsat 8 (L8) for water quality estimation has produced satisfactory results in many studies, for example in Mexico (González-Márquez et al., 2018) and China (Zheng et al., 2015). Similarly, Sentinel-2 (S2) data provided accurate estimates of WQPs for example in Brazil (Pompêo et al., 2021) and China (Liu et al., 2017). Despite the wider use of RS data in water quality studies, models relating satellite reflectance to in-situ WQP differed considerably. Thus, depending on location and the modelling technique, results of mixed accuracies have been obtained (Gholizadeh et al., 2016). This problem partly emanates from the inconsistency between studies regarding which spectral features or bands are useful for estimating the target parameter (Sagan et al., 2020). Generally, traditional linear regression (parametric) models have been used to construct functional relationships between parameters of water quality and reflectance data from satellite images (Coskun et al., 2008; Saadi et al., 2014; 2018). Nevertheless, machine learning (non-parametric) models such as random forests, support vector machines, neural networks etc. have been shown to provide better accuracies due to their ability to automatically learn from data, explain hidden patterns and non-linearity in reflectance data and optically-active WQPs (Naghibi et al., 2015; Prasad et al., 2020; Sagan et al., 2020). Hence, the suitability of satellite image data and modelling technique is of primary concern for the development of adaptive water quality monitoring capacity for the Owabi Dam. Additionally, the sole use of model-based for pixel-level prediction of WQPs to evaluate the status of water quality is largely uncertain, since the errors in the models can propagate to the population level. However, the combination of probability samples (from the sampling design) and the strength of the model can provide confident point estimates and spatio-temporal mapping of WQPs in the framework of model-assisted estimation (Gregoire, 1998; Särndal et al., 2003; Valentine et al., 2009).

The scope of this study is limited to the exploration of RS data particularly S2 and L8 for estimating water quality of the Owabi Dam reservoir, and to determine the current status of water quality. To achieve this, we assess the performance of three statistical models (random forests, support vector machines and linear regression) in retrieving water quality parameters of the Owabi Dam reservoir from S2 and L8 satellite imageries. The specific objectives were (i) to establish statistical relationships between remotely sensed data and water quality parameters; (ii) to construct a spatial distribution map of water quality parameters; and (iii) to estimate the status of water quality of the Owabi Dam reservoir.

2. Materials and methods

2.1. Study area

The Owabi Reservoir (Fig. 1) is located at 23 km northwest of Kumasi in the jurisdiction of the Kumasi Metropolitan Assembly

(KMA) on longitude 1° 42' N and latitude 6° 44' W (Akoto et al., 2017). The reservoir is centred in the Owabi Wildlife Sanctuary, an inner Ramsar site covering an area of about 13 km². The average area of the reservoir is 3.5 km² and it is drained by the following rivers: Owabi, Sukobri, Atafua, Akyeampomene, Pumpunase and Afu. To date, the reservoir is managed by the Ghana Water Company Limited (Owabi Headworks).

2.2. Field sampling design for the water quality assessment

The field water sampling was conducted in the dry season (23rd December 2019) using a systematic square grid design (Fig. 1) and assuming no marked variations in the flow direction. Initially, 47 sample points spaced evenly at 150 m apart in both north-south and east-west directions were generated in the Quantum-GIS environment (version 3.10.2). The location of each sample point on the reservoir was observed with a Garmin GPS (Garmin 65, Garmin®) with horizontal accuracy of 5 to 10 m under normal conditions.

At each point, surface water samples at a depth of 1 m were collected in a 10 m radius circular plot using labelled dry-rinsed plastic containers (Akoto et al., 2017). The samples were stored in an ice-box at a temperature of 4 °C, and further analysed for pH, turbidity, alkalinity, total dissolved solids (TDS) and dissolved oxygen (DO) at the laboratory of Owabi Headworks. The pH, TDS and DO were determined by potentiometry, turbidity was measured using turbidimeter, and titrimetric methods were used to determine the alkalinity. The laboratory analyses followed similar procedures of Boadi et al. (2018) and summary of the measured WQPs is given in Table 1.

2.3. Satellite data acquisition and processing

We utilized the S2 and L8 satellite imageries for the estimation of WQPs of the Owabi Dam reservoir. Image tiles with minimum cloud cover of less than 10%, covering the spatial extent of the reservoir and corresponding to the period of field water sampling were used. Level-1 data products of S2 and L8 were obtained freely from the earth explorer platform of the United States Geological Survey (<https://earthexplorer.usgs.gov>). The dates accessed for the datasets were 23rd December 2019 and 24th December 2019 for S2 and L8 respectively.

To achieve higher accuracies, pre-processing of image tiles such as atmospheric and geometric corrections were considered crucial in deriving significant relationships between field data and remotely sensed biophysical parameters (Copping, 2004; Appiah Mensah et al., 2019). The atmospheric correction was done by using the zero-brightness method, which involved the conversion of pixel values from digital numbers to surface reflectance values (Eq. (1)). The geometric correction was applied to correct for the topographic effects on the angular displacement of the sun (Eq. (2)).

$$S_R = B_M(D_N) + R_A \quad (1)$$

$$S_{TR} = \frac{S_R}{\sin(S_E)} \quad (2)$$

where S_R is the surface reflectance values after atmospheric correction; B_M denotes the band-specific multiplicative value; D_N is the digital number; R_A is the reflectance additive band value; S_{TR} is the surface reflectance values corrected for the sun angular displacement; and S_E is the sun elevation. Values of the above input parameters were extracted from the metadata files in the S2 and L8 image data.

The red-edge and short-wave-infrared bands of S2 were resampled to the native resolution (i.e. 10 m) using the bilinear

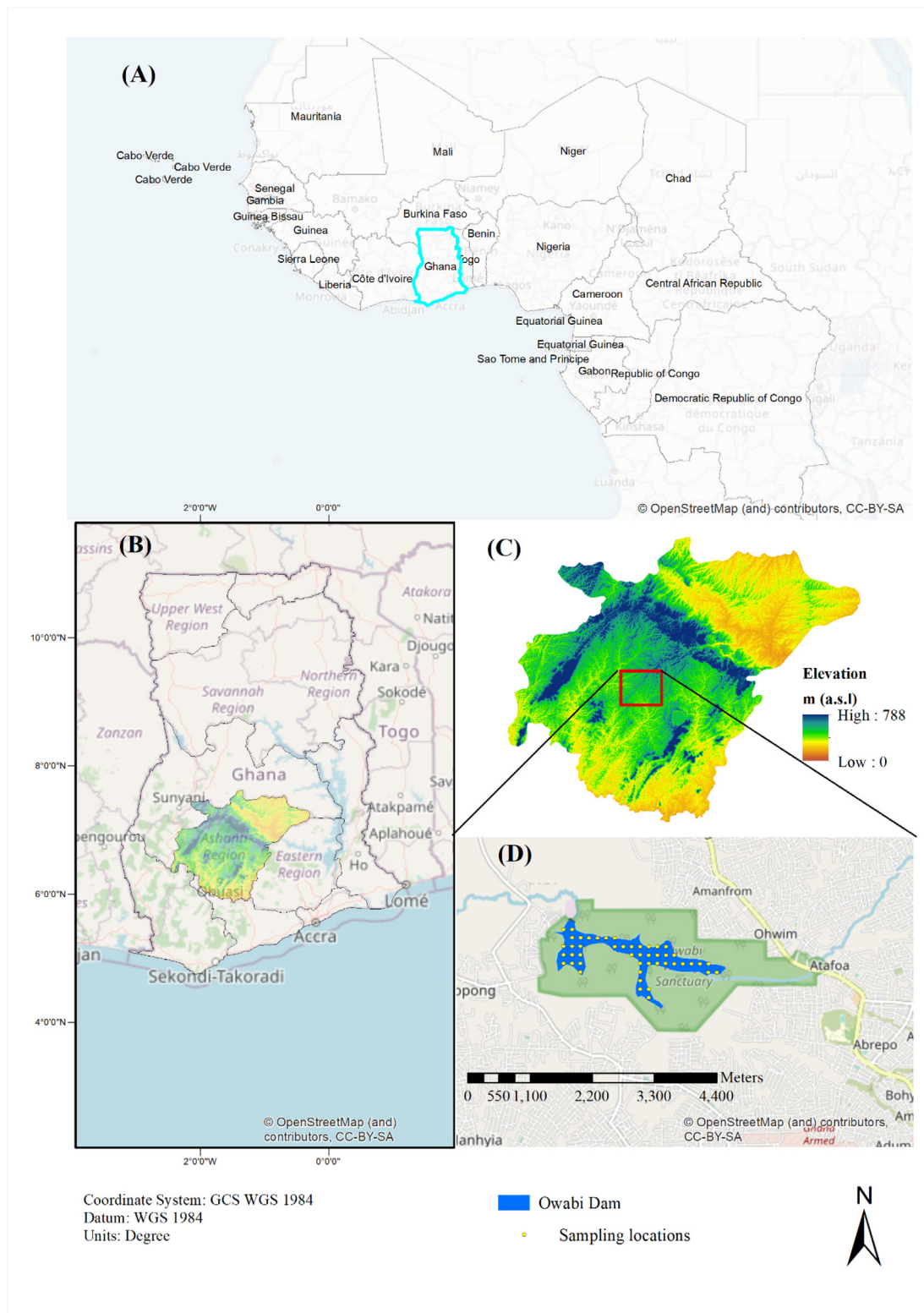


Fig. 1. The spatial location of (a) Ghana in West Africa, (b) the regional boundaries in Ghana, (c) the elevation of the study region and (d) Owabi Reservoir and the sampling sites.

interpolation technique. Using the sample plot coordinates, the spectral values of individual bands were extracted as area-weighted values (i.e. the average of pixel values within 10 m radius around the sample point) for each plot. The extraction was done using the ‘raster’ package in R (R Core Team, 2019). Two of the plots

had spectral values contaminated with clouds and so, were removed from the final dataset. The spectral bands of the two sensors consisting of the visible and infrared bands (Table A.1, Appendix, supplementary material) were used as predictors in the regression analyses.

Table 1

Summary statistics of measured WQPs of Owabi Reservoir. *Min* is minimum, *Max* is maximum, *Sd* is standard deviation, *Cv* is coefficient of variation and *n* is sample size.

WQP	*Statistics (n = 45)				
	Mean	Min	Max	Sd	Cv (%)
pH	7.06	6.74	7.90	0.26	3.68
Turbidity (mg/L)	33.21	31.94	40.13	1.72	5.18
Alkalinity (mg/L)	182.59	115.11	194.96	16.78	9.19
TDS (mg/L)	39.68	29.38	41.57	2.56	6.45
DO (mg/L)	3.92	3.83	4.40	0.12	3.06

*The statistics are computed from 45 samples instead of 47 due to presence of clouds in the spectral values of two sample locations.

2.4. Modelling the relationship between measured WQPs and spectral values

To establish statistical relationships between measured WQPs and remotely sensed spectral values for the Owabi Dam reservoir, three regression models were applied; a parametric, multiple linear regression (MLR) and two other non-parametric, random forests (RF) and support vector machine (SVM) models. All three models were fitted separately for S2 and L8 data and had a general formulation with the WQPs as response variables and the spectral bands as predictors. The model-specifics are described in the proceeding sections.

2.4.1. Multiple linear regression

To fit the MLR models, standard assumptions underlying linear regression analyses were evaluated based on tests of normality and variance homogeneity for each response variable using the Shapiro-Wilk and Fligner-Killeen’s tests in R, respectively. To avoid the issues of multicollinearity among the predictors, we used the information from both the Pearson product moment of correlation coefficient (*r*) and the variance inflation method (VIF) to remove highly correlated predictors. Predictor pairs with values of *r* > 0.6 and VIFs > 10 were excluded from the model. The MLR was fitted by the ordinary least squares method and was implicitly expressed as:

$$Y = \beta_0 + \beta_1 X_1 + \beta_2 X_2 + \dots + \beta_p X_p + \varepsilon \tag{3}$$

where *Y* is the (response variable); $\beta_0, \beta_1, \beta_2, \dots, \beta_p$ denote the regression parameters to be estimated; X_1, X_2, X_p are the remotely-sensed spectral bands; and ε is the independent and identically distributed errors with an expectation, $E(\varepsilon) = 0$ and a constant variance, $Var(\varepsilon) = \sigma^2$.

The significance of model parameters was tested at both 1% and 5% probability levels. During the MLR model fitting, predictors were included into the model by a stepwise approach (both ‘forward and backward’ selection) using the base packages of ‘caret’ and ‘MASS’ in R to enhance best model performance by lowering the estimation error (James et al., 2013).

2.4.2. Random forests

RF is a supervised ensemble-learning algorithm which has shown higher predictive performance in classification and regression analyses (Breiman, 2001). RF works by generating a set of decision trees that are aggregated to reduce the variance of predictions (i.e. overfitting). Among the predictor variables, the RF model was optimized by hyper-parameter tuning following similar procedures described by Li et al. (2017) and Abdi (2020). The RF model was fitted in R using the ‘randomforest’ package (R Core Team, 2019).

2.4.3. Support vector machines

The SVM searches for the optimum decision by generating decision boundaries (i.e. hyperplanes) in a feature space (Cortes and Vapnik, 1995). The SVM model was optimally parameterized

through a grid search for the best combination of ‘cost’ and ‘gamma’ values that minimized the error of prediction. In addition, the models were fitted through radial kernel function in the ‘e1071’ package (R Core Team, 2019) to account for the non-linearity of the spectral bands (Abdi, 2020).

2.4.4. Accuracy assessment of regression models

To evaluate the accuracy of the fitted models, repeated k-fold cross-validation technique was applied. This was considered appropriate due to the smaller number of observations (*n* = 45) which could not allow for a split into training and testing datasets. The cross-validation was done using 10 random subsets across three repetitions (*k* = 10) and recorded the prediction error after each iteration. The averages of the k-recorded errors were summarized using the accuracy metrics (Eqs. (4)–(6)): the adjusted coefficient of determination (R^2_{adj}), root mean square error (RMSE), and the prediction error rate (PE).

$$R^2_{adj} = 1 - \frac{(n - 1) \sum_{i=1}^n (\hat{y}_i - y_i)^2}{(n - p) \sum_{i=1}^n (\hat{y}_i - \bar{y}_i)^2} \tag{4}$$

$$RMSE = \sqrt{\frac{\sum_{i=1}^n (\hat{y}_i - y_i)^2}{n - p}} \tag{5}$$

$$PE = 100\% \times \frac{RMSE}{\bar{y}} \tag{6}$$

where \hat{y}_i, y_i and \bar{y}_i are the predicted, measured and average values of the dependent variable, respectively; *n* represents the total number of observations used for fitting the model; and *p* denotes the number of model parameters. The prediction error rate (PE) was further used to compare inter-sensor relative efficiencies between the S2- and L8-predicted WQPs under the three models.

2.5. Mapping and estimation of WQPs for Owabi Dam reservoir

The best performing model (based on the accuracy metrics) and sensor were used to construct a 10 m spatial resolution map of WQPs for the entire Owabi Reservoir. To compute an estimator (mean of each WQP) for the reservoir, we applied the generalised model-assisted estimators (Särndal et al., 2003). The map-based estimate for each WQP in the Owabi Reservoir was computed as:

$$\hat{\mu}_{map} = \frac{1}{N} \sum_{j=1}^N \hat{y}_j \tag{7}$$

where *N* was the number of 10 m × 10 m population units (pixels) in the study area and \hat{y}_j is the model prediction for the *i*-th map unit. The map-based estimate ($\hat{\mu}_{map}$) was adjusted for systematic model prediction errors from the field sample as:

$$\hat{Bias}_{(\hat{\mu}_{map})} = \frac{1}{n} \sum_{i=1}^n (\hat{y}_i - y_i) \tag{8}$$

where n is the sample size of the field plots ($n = 45$); \hat{y}_i is the model prediction for the i -th sample unit; and y_i is the observed value for i -th sample unit. Subsequently, the model-assisted estimator for the mean of each WQP was derived as:

$$\hat{\mu}_{mod-assisted} = \hat{\mu}_{map} - \widehat{Bias}_{(\hat{\mu}_{map})} \quad (9)$$

The corresponding standard error of the $\hat{\mu}_{mod-assisted}$ was computed as:

$$SE_{(\hat{\mu}_{mod-assisted})} = \sqrt{\frac{1}{n(n-1)} \sum_{i=1}^n (e_i - \bar{e})^2} \quad (10)$$

where e_i is the residual error estimated as the difference between the observed (y_i) and predicted (\hat{y}_i) i -th values and \bar{e} is the mean of the residuals. Finally, the estimated WQPs ($\hat{\mu}_{mod-assisted}$) for the entire study area were compared to the World Health Organization reference values (World Health Organization, 2006) to characterize the surface water quality status of the Owabi Dam reservoir.

3. Results

3.1. Relationships between spectral reflectance and field measured WQPs

The accuracies of the three models for the two sensors are presented in Table 2. Regardless of the sensor, RF produced the greatest accuracies for all WQPs. Generally, the accuracies achieved under S2 were superior to L8. For S2, the explained variance (R^2 , adj) was highest for RF and ranged between 0.95 and 0.99, followed closely by the SVM (0.94–0.98) and least for the MLR (0.55–0.91). For L8, satisfactory accuracies were obtained from the RF model (0.82–0.86), and the MLR showed a moderate performance (0.33–0.42), while the SVM exhibited the poorest results (0.13–0.23). The relative prediction errors of the two sensors under all three models showed that S2 outperforms L8 on average by 63% (RF), 65% (MLR) and 75% (SVM). The prediction uncertainty was largest in the estimates of alkalinity and lowest for those of dissolved oxygen.

The parameter estimation from the MLR models of both S2 and L8 is given in Table 3. For L8, the red, blue and green spectral bands were key predictors in each WQP, while the green spectral band was the only visible band important for the S2 models. However, with the exception of dissolved oxygen, the red-edge bands were also key predictors in the S2 models under MLR (Table 3) and RF (Fig. 2).

The relationships between the observed and predicted WQPs for both S2 and L8 by the three models are shown in Fig. 3. Regardless of the model used, the observed and predicted values agreed strongly well for S2 compared to L8. However, the predictions around the mean corresponded well for the two sensors. The L8 showed stronger underestimation at larger values of pH, turbidity

and dissolved oxygen and overestimation at lower levels of alkalinity and total dissolved solids. These discrepancies in L8 predictions were largest for the SVM, followed by the MLR and least for the RF.

The residuals of the RF model indicated absence of heteroscedastic patterns in the studied WQPs (Fig. A.2). The RF model and S2 were selected for the spatial prediction and mapping of WQPs of the Owabi Dam reservoir.

3.2. Mapping and estimation of WQPs for the entire Owabi Dam reservoir

The RF model and S2 data were used to predict spatial WQPs for each of the 10,702 10×10 m resolution WQP target units in the study area as presented in Fig. 4. Predictions of pH ranged between 6.75 and 7.63, with a model-assisted mean estimate of 7.06. The corresponding map predictions range (and mean) were 32.0–38.65 (33.49 mg/L) for turbidity, 130.41–194.35 (179.60 mg/L) for alkalinity, 31.51–41.48 (39.19 mg/L) for total dissolved solids, and 3.84–4.30 (3.94 mg/L) for the dissolved oxygen. The corresponding estimated standard errors for the predicted map units were also very small (<0.0001). Comparison of the mean estimates of each WQP with the WHO reference limits indicated that the pH, total dissolved solids and alkalinity were within acceptable limits, except for the turbidity which was higher than normal (Table 4).

4. Discussion

The aim of this study was to explore the feasibility of S2 and L8 in the retrieval of WQP of the Owabi Dam. Higher accuracies obtained from the tested models indicated parameters of water quality could be derived from spectral reflectance data. We obtained higher accuracies with the machine learning models (RF and SVM) than for the traditional linear regression models. Similarly, using machine learning models, Naghibi et al. (2015) and Prasad et al. (2020) found 71% and 94% accuracies with the RF for mapping potential groundwater in Iran and India, respectively. Others such as deep learning has been found to provide higher estimates of water quality retrieval in the United States (Sagan et al., 2020). Abdi (2020) and Peterson et al. (2019) suggested that the general better performance of machine learning models with RS data compared to parametric models is that machine learning models enable higher-level and non-linear statistical relations to be uncovered. Nevertheless, sufficient accuracies of water quality retrieval could also be obtained from a well-formulated parametric model as demonstrated by (Adelmalik, 2016; Gholizadeh and Melesse, 2017).

As expected, differences in spatial and spectral resolution had a stronger effect on the accuracy of WQP retrieval under S2 and L8. We obtained higher accuracies for S2 than for L8 (Table 2). The spatial resolution of S2 (10 m) is three times higher than L8 (30 m) and thus, L8 might be more heterogeneous in terms of spectral reflectance thereby reducing its accuracy. In the spectral domain, S2 offers

Table 2
Repeated cross-validation accuracy statistics of MLR, RF and SVM models for WQPs under S2 and L8.

WQP	MLR						RF						SVM					
	S2			L8			S2			L8			S2			L8		
	R ² .adj	RMSE	PE	R ² .adj	RMSE	PE	R ² .adj	RMSE	PE	R ² .adj	RMSE	PE	R ² .adj	RMSE	PE	R ² .adj	RMSE	PE
pH	0.87	0.09	1.27	0.42	0.21	2.97	0.95	0.07	0.99	0.86	0.12	1.70	0.94	0.07	0.99	0.23	0.24	3.40
Turbidity (mg/L)	0.91	0.34	1.02	0.33	1.48	4.46	0.99	0.29	0.87	0.82	0.90	2.71	0.98	0.41	1.23	0.13	1.67	5.03
Alkalinity (mg/L)	0.89	3.14	1.72	0.39	13.85	7.59	0.99	3.03	1.66	0.84	8.31	4.55	0.98	3.99	2.19	0.13	16.29	8.92
TDS (mg/L)	0.55	1.32	3.33	0.39	2.16	5.44	0.99	0.45	1.13	0.83	1.32	3.33	0.97	0.61	1.54	0.14	2.49	6.28
DO (mg/L)	0.87	0.03	0.77	0.35	0.10	2.55	0.98	0.02	0.51	0.82	0.06	1.53	0.98	0.03	0.77	0.14	0.12	3.06
Rel-PE (%)	64.79						62.68						74.91					

Table 3
Parameter estimates from the multiple linear regression models of WQPs. Values in parenthesis are estimated standard errors.

WQP	Sentinel-2 (S2)		Landsat-8 (L8)	
	Spectral bands	Estimate	Spectral bands	Estimate
pH	Intercept	6.32 (0.08)	Intercept	11.61 (5.67)
	Green	23.53 (2.47)	Green	118.36 (82.13)
	RE2	-5.42 (2.28)	Blue	-56.62 (44.54)
	RE4	3.46 (1.45)	Red	4.68 (98.35)
	NIR	-1.87 (0.87)	SWIR2	-23.67 (13.93)
	SWIR2	6.53 (2.83)		
Turbidity	Intercept	28.50 (0.23)	Intercept	107.03 (29.93)
	Green	142.47 (8.02)	Green	-96.86 (341.75)
	RE3	-16.80 (1.80)	Blue	-72.22 (276.15)
	SWIR2	50.82 (9.92)	Red	637.59 (545.42)
Alkalinity	Intercept	229.40 (2.21)	Intercept	-218.10 (383.9)
	Green	-1332.70 (82.81)	Green	-4731.17 (5569.7)
	RE4	146.74 (15.79)	Blue	1072.30 (3020.2)
	SWIR2	-534.70 (101.19)	Red	-1049.30 (6669.5)
Total dissolved solids	Intercept	40.26 (0.49)	Intercept	1195.70 (944.4)
	RE2	80.82 (8.61)	Green	-21.47 (58.63)
	SWIR2	302.33 (29.89)	Blue	-721.96 (850.56)
			Red	163.42 (461.23)
Dissolved oxygen	Intercept	3.53 (0.02)	Red	-160.03 (1018.52)
	Green	11.95 (0.47)	SWIR2	182.47 (144.22)
	NIR	-0.89 (0.17)	Intercept	6.38 (3.21)
	SWIR1	0.73 (0.35)	Green	38.74 (17.28)
			Blue	-6.77 (20.97)
		NIR	0.24 (4.23)	
		SWIR2	-10.27 (20.92)	

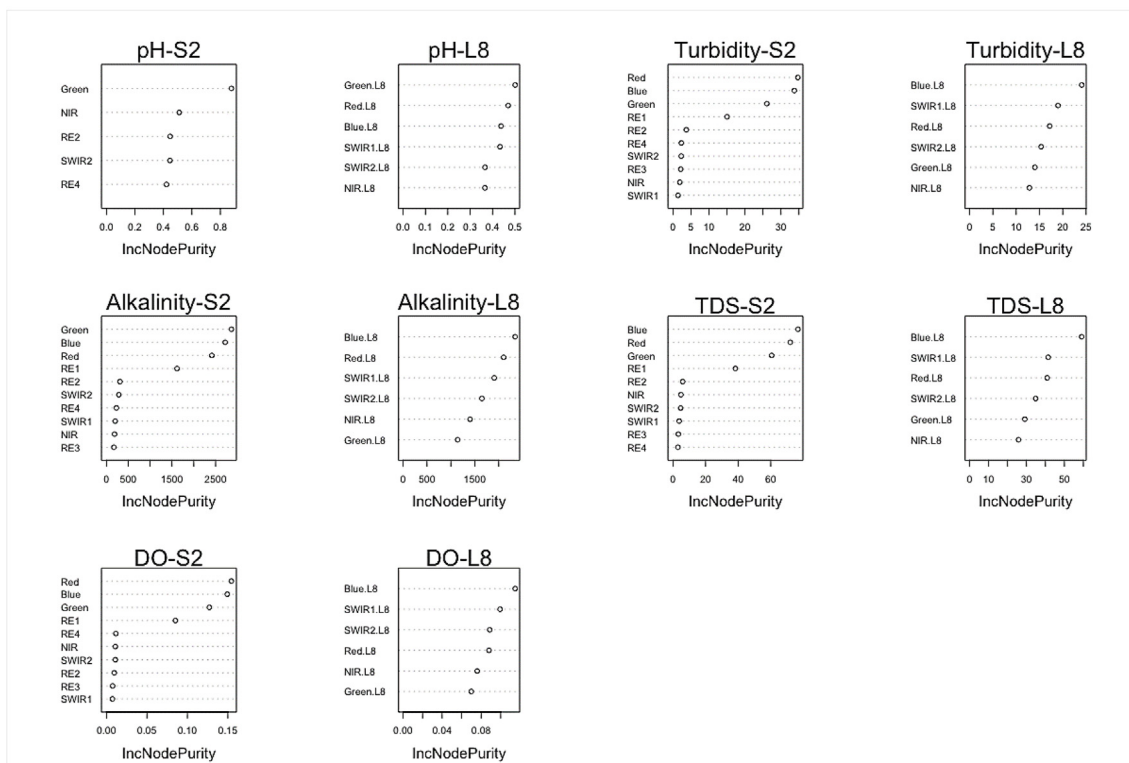


Fig. 2. Importance of spectral bands in estimating WQPs from Sentinel-2 (S2) and Landsat 8 (L8) using random forest model (RF).

more spectral bands than L8, particularly, the presence of red-edge bands. Together with the visible and infra-red bands, the red-edge bands were also key predictors in the S2 models under MLR and RF for all WQPs except dissolved oxygen (Table 3 and Fig. 2). Mollae (2018) used the red-edge bands for accurate detection and mapping of chlorophyll content and phytoplankton in the Western Basin of Lake Erie, and Liu et al. (2017) and Pompêo et al. (2021) found significant contributions in estimating WQPs using both the visible and

red-edge bands for in Brazil and China, respectively. Another reason for the difference could be the plot design used for water sampling in our study, water samples were collected within a 10 m radius around the sampling point which is more or less the same spatial resolution of S2. Nevertheless, the L8 provided satisfactory accuracy and predicted strongly well around the means of the various WQPs. For example, by using Landsat 5 and 8 imageries, Gholizadeh and Melesse (2017) obtained an R² of 84% for turbidity, which was sim-

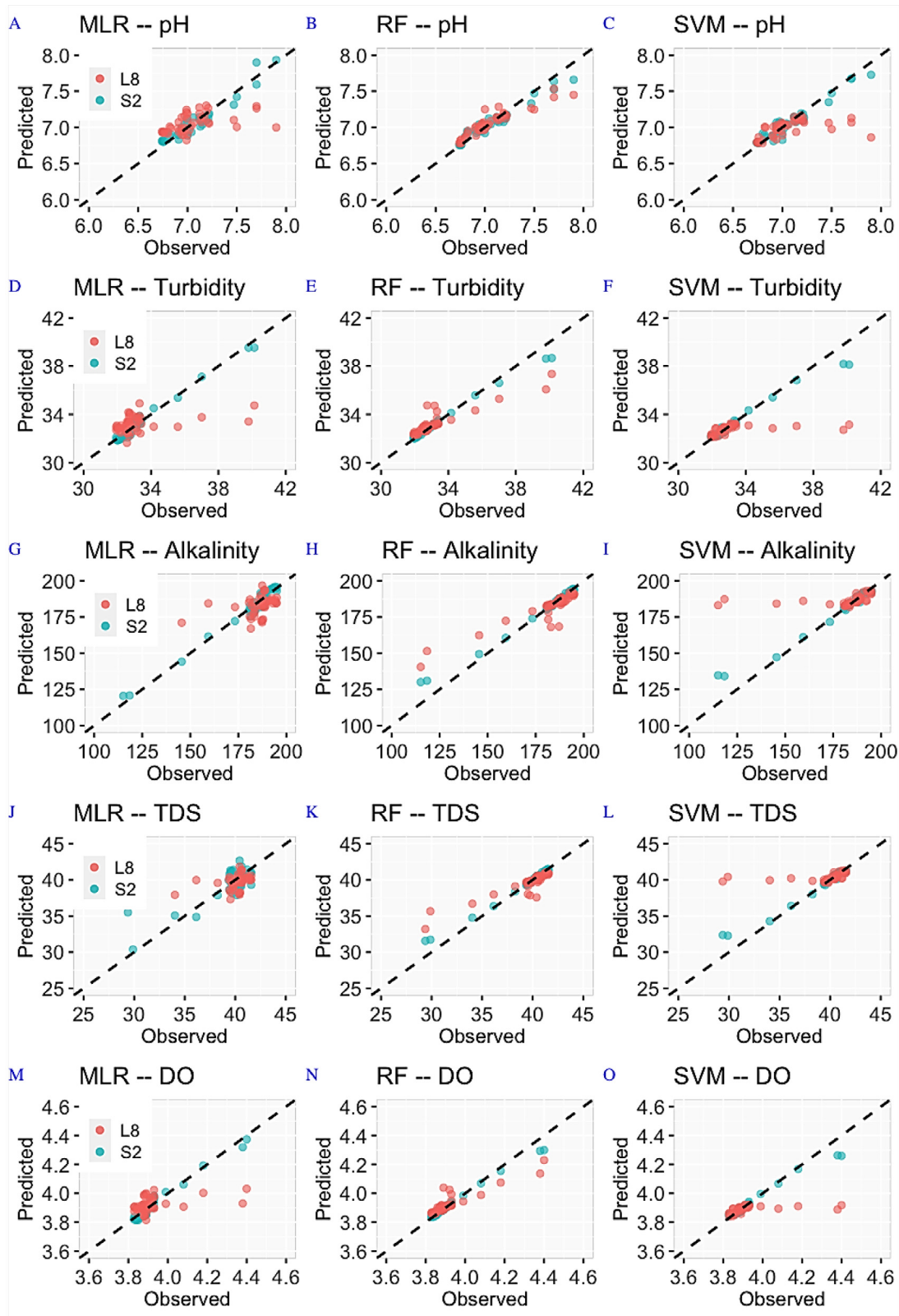


Fig. 3. Observed versus predicted values using MLR, RF and SVM models on S2 and L8 data for pH (A-C), turbidity (D-F), alkalinity (G-I), total dissolved solids (J-L) and dissolved oxygen (M–O). The diagonal dashed-line shows a 1:1 relation.

ilar to our result for L8 under RF ($R^2 = 82\%$). Further, the use of L8 for water quality estimation has also produced satisfactory results in many studies, for example in Mexico (González-Márquez et al., 2018) and China (Zheng et al., 2015). Compared to S2, Landsat has

a long history allowing for spatio-temporal trends assessment of water quality (Saadi et al., 2014; Gholizadeh et al., 2016). Additionally, the 16-day repeat cycle as well as the availability of panchromatic band (15 m) of L8 can equally facilitate monitoring of water

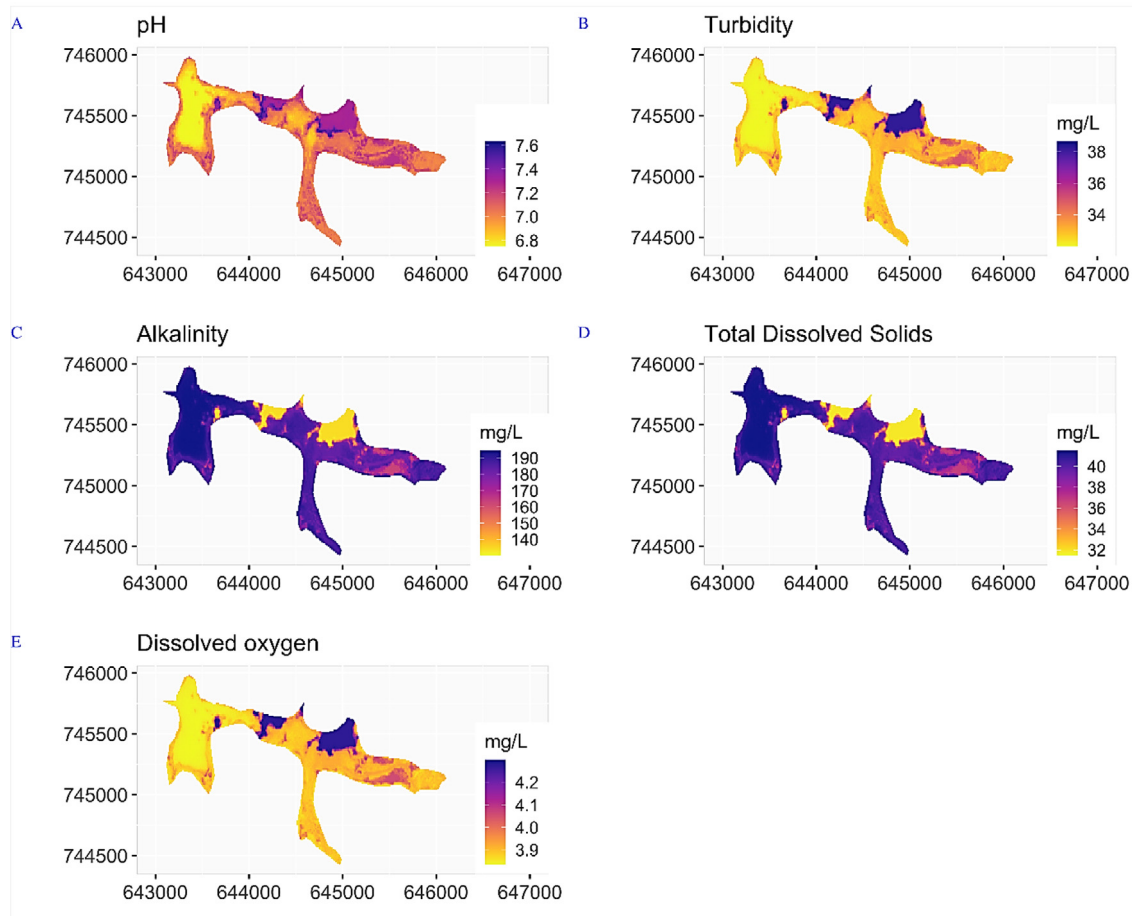


Fig. 4. Generated 10 m spatial water quality maps of the Owabi Reservoir using the RF model and S2 satellite data.

Table 4 Model-adjusted map estimate of WQPs and comparison with WHO standards (2006).

WQPs	$\hat{\mu}_{mod-assisted}$ (range)	$SE(\hat{\mu}_{mod-assisted})$	WHO reference
pH	7.06 (6.75–7.63)	5.57×10^{-17}	6.50–8.50
Turbidity (mg/L)	33.49 (32.00–38.65)	1.65×10^{-16}	5.00
Alkalinity (mg/L)	179.60 (130.41–194.35)	1.97×10^{-15}	200.00
TDS (mg/L)	39.19 (31.51–41.48)	4.66×10^{-16}	1000.00
DO (mg/L)	3.94 (3.84–4.30)	3.43×10^{-18}	–

quality with a greater detail. We propose also that L8 can be used in tandem with S2 to monitor the water quality of Owabi Dam reservoir. It is also worth to mention that spatial features derived from texture metrics on the basis of the radiometric resolution could enhance better retrieval of optical WQPs. However, these were not considered in our study due to the low signal-to-noise ratio of moderate L8 and S2 which prevents the use of spectral shape algorithms and bio-optical inversion estimators (Sagan et al., 2020).

The range of predicted WQPs were similar to recent studies done on the area (Akoto et al., 2017; Boadi et al., 2018) but showed increasing trends when compared to Akoto et al. (2008). However, similar study is needed for the wet season to ascertain for spatio-temporal trends in water quality of Owabi Dam.

5. Conclusion

The study has shown that WQPs of Owabi Dam can be retrieved from satellite imageries with high accuracies. S2 and the RF model are most suitable for estimating and wall-to-wall mapping of WQPs of the Dam, though L8 can also be used in tandem. The

developed models have the potential to be used in empirical and process-based water quality forecasting models under given climate change scenarios and for the development of integrated water resources management plan for the reservoir. It is envisioned that incorporating satellite data in WQP estimation will not only reduce cost during field sampling, but also enhance sustainable monitoring of the Owabi Dam reservoir in a consistent and resource-efficient way.

Declaration of Competing Interest

The authors declare that they have no known competing financial interests or personal relationships that could have appeared to influence the work reported in this paper.

Appendix A. Supplementary data

Supplementary data to this article can be found online at <https://doi.org/10.1016/j.ejrs.2021.06.006>.

References

Abdelmalik, K.W., 2018. Role of statistical remote sensing for Inland water quality parameters prediction. *Egypt. J. Remote Sens. Space Sci.* 21, 193–200. <https://doi.org/10.1016/j.ejrs.2016.12.002>.
 Abdi, A.M., 2020. Land cover and land use classification performance of machine learning algorithms in a boreal landscape using Sentinel-2 data. *GIScience Remote Sens.* 57, 1–20. <https://doi.org/10.1080/15481603.2019.1650447>.
 Akoto, O., Abankwa, E., 2014. Evaluation of Owabi Reservoir (Ghana) water quality using factor analysis. *Lakes Reservoirs: Sci., Policy Manage. Sustain. Use* 19, 174–182. <https://doi.org/10.1111/lre.12066>.

- Akoto, O., Bruce, T.N., Darko, D., 2008. Heavy metals pollution profiles in streams serving the Owabi reservoir. *Afr. J. Environ. Sci. Technol.* 2, 354–359. <https://doi.org/10.4314/ajest.v2i11>.
- Akoto, O., Gyamfi, O., Darko, G., Barnes, V.R., 2017. Changes in water quality in the Owabi water treatment plant in Ghana. *Appl. Water Sci.* 7, 175–186. <https://doi.org/10.1007/s13201-014-0232-4>.
- Appiah Mensah, A., Akoto Sarfo, D., Partey, S.T., 2019. Assessment of vegetation dynamics using remote sensing and GIS: a case of Bosomtwe Range Forest Reserve, Ghana. *Egypt. J. Remote Sens. Space Sci.* 22, 145–154. <https://doi.org/10.1016/j.ejrs.2018.04.004>.
- Badu, M., Wemegah, D.D., Boadi, N.O., Brown, F.A., 2013. Assessment of the Nutrient Load and Selected Heavy Metals in the Owabi Reservoir and its Feeder Waters. *American Journal of Scientific and Industrial Research*, Science Huß, ISSN: 2153-649X, doi:10.5251/ajsir.2013.4.4.337.343
- Boadi, N.O., Borquaye, L.S., Darko, G., Wemegah, D.D., Agorsor, D., Akrofi, R., 2018. Assessment of the quality of the Owabi reservoir and its tributaries. *Cogent Food Agric.* 4, 1492360. <https://doi.org/10.1080/23311932.2018.1492360>.
- Breiman, L., 2001. Random forests. *Machine Learning* 45, 5–32. <https://doi.org/10.1023/A:1010933404324>.
- Copping, J., 2004. Digital change detection methods in ecosystem monitoring: a review. *Int. J. Remote Sens.* 25, 1565.
- Cortes, C., Vapnik, V., 1995. Support-vector networks. *Mach. Learn.* 20, 273–297. <https://doi.org/10.1007/BF00994018>.
- Coskun, H.G., Tanik, A., Alganci, U., Cigizoglu, H.K., 2008. Determination of environmental quality of a drinking water reservoir by remote sensing, GIS and regression analysis. *Water Air Soil Pollut.* 194, 275–285. <https://doi.org/10.1007/s11270-008-9716-x>.
- Du Laing, G., Rinklebe, J., Vandecasteele, B., Meers, E., Tack, F.M.G., 2009. Trace metal behaviour in estuarine and riverine floodplain soils and sediments: A review. *Science of The Total Environment*, Thematic Papers: Selected papers from the 2007 Wetland Pollutant Dynamics and Control Symposium 407, 3972–3985. DOI:10.1016/j.scitotenv.2008.07.025.
- Feyisa, G.L., Meilby, H., Fensholt, R., Proud, S.R., 2014. Automated water extraction index: A new technique for surface water mapping using Landsat imagery. *Remote Sens. Environ.* 140, 23–35. <https://doi.org/10.1016/j.rse.2013.08.029>.
- Gholizadeh, M.H., Melesse, A.M., Reddi, L., 2016. A comprehensive review on water quality parameters estimation using remote sensing techniques. *Sensors* 16, 1298. <https://doi.org/10.3390/s16081298>.
- Gholizadeh, M., Melesse, A., 2017. Study on spatiotemporal variability of water quality parameters in Florida Bay using remote sensing. *J. Remote Sens. GIS* 6, 2.
- González-Márquez, L.C., Torres-Bejarano, F.M., Rodríguez-Cuevas, C., Torregroza-Espinosa, A.C., Sandoval-Romero, J.A., 2018. Estimation of water quality parameters using Landsat 8 images: application to Playa Colorada Bay, Sinaloa, Mexico. *Appl. Geomat.* 10, 147–158. <https://doi.org/10.1007/s12518-018-0211-9>.
- Gregoire, T.G., 1998. Design-based and model-based inference in survey sampling: appreciating the difference. *Can. J. For. Res.* 28, 1429–1447. <https://doi.org/10.1139/x98-166>.
- James, G., Witten, D., Hastie, T., Tibshirani, R., 2013. *An Introduction to Statistical Learning*. Springer Texts in Statistics. Springer New York, New York, NY. DOI:10.1007/978-1-4614-7138-7.
- Karikari, A.Y., Bernasko, J.K., Bosque-Hamilton, E.K.A., 2007. An assessment of water quality of Angaw River in Southeastern Coastal Plains of Ghana. *West Afr. J. Appl. Ecol.* 11. <https://doi.org/10.4314/wajae.v11i1.45728>.
- Li, Z., Xin, X., Tang, H., Yang, F., Chen, B., Zhang, B., 2017. Estimating grassland LAI using the Random Forests approach and Landsat imagery in the meadow steppe of Hulunber, China. *J. Integr. Agric.* 16, 286–297. [https://doi.org/10.1016/S2095-3119\(15\)61303-X](https://doi.org/10.1016/S2095-3119(15)61303-X).
- Liu, H., Li, Q., Shi, T., Hu, S., Wu, G., Zhou, Q., 2017. Application of Sentinel 2 MSI images to retrieve suspended particulate matter concentrations in Poyang Lake. *Remote Sens.* 9, 761. <https://doi.org/10.3390/rs9070761>.
- Marobhe, N.J., Renman, G., Jacks, G., 2007. The study of water supply and traditional water purification knowledge in selected rural villages in Tanzania. *Indigenous knowledge systems and sustainable development: relevance for Africa. Tribes Tribals* 1, 111–120.
- Mollae, S., 2018. Estimation of Phytoplankton Chlorophyll-a Concentration in the Western Basin of Lake Erie Using Sentinel-2 and Sentinel-3 Data. Master thesis. University of Waterloo. <https://uwaterloo.ca/handle/10012/13456>. Accessed 20/02/2020.
- Naghbi, S.A., Pourghasemi, H.R., Dixon, B., 2015. GIS-based groundwater potential mapping using boosted regression tree, classification and regression tree, and random forest machine learning models in Iran. *Environ. Monit. Assess.* 188, 44. <https://doi.org/10.1007/s10661-015-5049-6>.
- Ntow, W.J., 2001. Organochlorine pesticides in water, sediment, crops, and human fluids in a farming community in Ghana. *Arch. Environ. Contam. Toxicol.* 40, 557–563. <https://doi.org/10.1007/s002440010210>.
- Peterson, K.T., Sagan, V., Sidike, P., Hasenmueller, E.A., Sloan, J.J., Knouft, J.H., 2019. Machine learning-based ensemble prediction of water-quality variables using feature-level and decision-level fusion with proximal remote sensing. *Photogramm. Eng. Remote Sens.* 85, 269–280. <https://doi.org/10.14358/PERS.85.4.269>.
- Pompêo, M., Moschini-Carlos, V., Bitencourt, M.D., Sôria-Perpinyà, X., Vicente, E., Delegido, J., 2021. Water quality assessment using Sentinel-2 imagery with estimates of chlorophyll a, Secchi disk depth, and Cyanobacteria cell number: the Cantareira System reservoirs (São Paulo, Brazil). *Environ Sci Pollut Res.* DOI:10.1007/s11356-021-12975-x.
- Prasad, P., Lovesson, V.J., Kotha, M., Yadav, R., 2020. Application of machine learning techniques in groundwater potential mapping along the west coast of India. *GIScience Remote Sens.*, 1–18 <https://doi.org/10.1080/15481603.2020.1794104>.
- R Core Team, 2019. *R: A language and environment for statistical computing*. R Foundation for Statistical Computing, Vienna, Austria. <https://www.R-project.org/>.
- Saadi, A.M.E., Yousry, M.M., Jahin, H.S., 2014. Statistical estimation of Rosetta branch water quality using multi-spectral data. *Water Sci.* 28, 18–30. <https://doi.org/10.1016/j.wsj.2014.10.001>.
- Sagan, V., Peterson, K.T., Maimaitijiang, M., Sidike, P., Sloan, J., Greeling, B.A., Maalouf, S., Adams, C., 2020. Monitoring inland water quality using remote sensing: potential and limitations of spectral indices, bio-optical simulations, machine learning, and cloud computing. *Earth Sci. Rev.* 205. <https://doi.org/10.1016/j.earscirev.2020.103187>.
- Särndal, C.-E., Swensson, B., Wretman, J., 2003. *Model Assisted Survey Sampling*. Springer Science & Business Media.
- United Nations world water assessment programme, 2009. *The United Nations world water development report 3: Water in a changing world*. Unesco, Paris and Earthscan, London. <http://webworld.unesco.org/water/wwap/wwdr/wwdr3/>.
- Usharani, K., Umarani, K., Ayyasamy, P., Shanthi, K., Lakshmanaperumalsamy, P., 2010. Physico-chemical and bacteriological characteristics of Noyyal River and ground water quality of Perur, India. *J. Appl. Sci. Environ. Manage.* 14.
- Valentine, H.T., Affleck, D.L.R., Gregoire, T.G., 2009. Systematic sampling of discrete and continuous populations: sample selection and the choice of estimator. *Can. J. For. Res.* 39, 1061–1068. <https://doi.org/10.1139/X09-019>.
- World Health Organization Guidelines for Drinking Water Quality Recommendations vol. 1 3rd Edition. 2004 Geneva, Switzerland. Accessed 2/24/2020.
- World Health Organization, 2006. *Guidelines for drinking-water quality: Incorporating the first and second addenda*. Geneva: Switzerland. Accessed 2/24/2020.
- Zheng, Z., Li, Y., Guo, Y., Xu, Y., Liu, G., Du, C., 2015. Landsat-based long-term monitoring of total suspended matter concentration pattern change in the wet season for Dongting Lake, China. *Remote Sens.* 7, 13975–13999. <https://doi.org/10.3390/rs71013975>.